

Exploring the Chemistry of Re^I : Physical and Theoretical Investigations

by

Philip D. Bulsink

*Thesis submitted to the
Faculty of Graduate and Postdoctoral Studies
In partial fulfilment of the requirements
For the degree of*

***Master of Science
In
Chemistry***

*Ottawa-Carleton Chemistry Institute
University of Ottawa*

Supervisors: *Professors Darrin Richeson & Tom Woo*

© Philip D. Bulsink, Ottawa, Canada, 2014

Abstract

The development of Rhenium I photocatalysts has been pursued since Lehn first showed the excellent performance of the Re^{I} bipyridine tricarbonyl catalyst. Since then, development has modified the organic ligand to demonstrate continued or improved activity with other α -diimine bidentate geometries. Geometry has been limited to κ_2 motifs, with *fac*-(CO)₃ and axial halide. This work will demonstrate the synthesis, characterization, and testing of a new $\kappa_3(\text{L}_3)\text{-Re}^{\text{I}}\text{-mer}(\text{CO})_2\text{X}$ (X = Cl, Br, CN, OTf) family of compounds for CO₂ reduction, as well as computational investigations into the mechanism of the reduction,

Acknowledgements

Thanks to the members of the Richeson and Woo research groups, both past and present, for the assistance provided and for making the time spent researching and writing this thesis enjoyable. Thanks as well to Frank and Sean in the Brusso lab, for their willingness to allow use of their characterization equipment. Thanks to Jake and the Gambarotta laboratory for use of their GC, and to the Sciano Lab, especially Janice, Charles, and Deni, for the use of their photolysis equipment.

I'd like to thank Dr. Ilia Korobkov for his work measuring and solving the x-ray crystal structures of the compounds discussed. He assisted with some paper writing as well.

Finally, I'd like to thank my fiancé Leanne, and my parents for their unending support, and understanding when I came home frustrated or exhausted from work.

Contents

1	Introduction	1
1.1	Inorganic Chemistry	1
1.2	Photochemistry & Catalysis	2
1.3	Rhenium	3
2	New Coordination Geometries for Re^I	7
2.1	Introduction	7
2.2	Synthesis of Bidentate and Terdentate Re ^I Complexes	8
2.3	Characterization	11
2.3.1	NMR Analysis	11
2.3.2	X-Ray Crystallography	13
2.3.3	Infrared Spectroscopy	24
2.3.4	Photophysical Properties	24
2.4	Conclusions	27
3	Photocatalysis of CO₂	28
3.1	Introduction	28
3.2	Photocatalytic Reactions with New Compounds	29
3.2.1	Conditions	29
3.2.2	Experimental Results	29
3.3	Section	30
3.4	Section	30
3.4.1	Subsection	30
4	Mechanism of CO₂ Reduction	31
4.1	Introduction	31
4.2	Literature Mechanisms	32

4.3	Consequences From κ^2 Terpyridine Complex Inactivity	33
4.4	Comparison Between Mechanistic Pathways	34
4.4.1	Subsection	34
5	Conclusions	35
A	Experimental Procedures	36
A.1	General Methods	36
A.2	Computational Methods	37
A.3	X-ray Crystallography	38
A.3.1	X-Ray Structures from Multiple Vantage Points	39
A.4	(terpy- κ^2 -N,N')Re(CO) ₃ Cl (1)	40
A.5	(terpy- κ^3 -N,N',N'')Re(CO) ₂ Cl (2)	40
A.6	(terpy- κ^2 -N,N')Re(CO) ₃ Br (3)	41
A.7	(terpy- κ^3 -N,N',N'')Re(CO) ₂ Br (4)	41
A.8	(terpy- κ^2 -N,N')Re(CO) ₃ OTf (7)	41
A.9	(terpy- κ^3 -N,N',N'')Re(CO) ₂ OTf (8)	42
B	Molecular Orbitals and Energy Diagrams	44
	Glossary of Terms	45

List of Tables

2.1	Selected Distances, Angles, and Torsions for 1	18
2.2	Selected Distances, Angles, and Torsions for 3	19
2.3	Selected Distances, Angles, and Torsions for 5	20
2.4	Crystal data and structure refinement for compounds 1 , 3 , 5 , and 7 . . .	22
2.5	Crystal data and structure refinement for compounds 2 , 4 , 6 , and 8 . . .	23

List of Figures

1.1	Two common bidentate complexes using terdentate ligands	4
2.1	Results of TGA analysis on 1 and 3	9
2.2	The aromatic region of the ^1H NMR spectra of 3 bidentate compounds .	12
2.3	The aromatic region of the ^1H NMR spectra showing bidentate - terdentate conversion	13
2.4	Proton-explicit skeletal drawing of 2,2':6',2''-terpyridine	13
2.5	X-ray crystal structure representation for 1	14
2.6	X-ray crystal structure representation for 3	15
2.7	X-ray crystal structure representation for 5	15
2.8	X-ray crystal structure representation for 2	17
2.9	X-ray crystal structure representation for 8	21
2.10	FTIR Spectra for complexes 1 and 2	25
2.11	Spectra for compounds 1 , 3 , 5 , and 7	26
2.12	Spectra for compounds 2 , 4 , 6 , and 8	26
2.13	UV-Vis spectra for all compounds	26
4.1	Overview of mechanistic pathways	32
4.2	Reaction energies for three mechanistic pathways	34
B.1	UV-Vis1	44

Chapter 1

Introduction

1.1 Inorganic Chemistry

Common distinctions split most chemical compounds into one of two categories: organic and inorganic. Organic molecules contain carbon and hydrogen, with or without additional nitrogen, oxygen, phosphorus, sulfur, and the halides. Inorganic chemistry is, therefore, considered to be the remainder of the molecules possible. While they may include some aspect of organic chemistry (especially in organometallic molecules), the main structural motif or reactive center is a non-organic feature. These inorganic compounds can range from compounds such as lithium or grignard reagents with significant organic influence, to metallic alloys or mineral compounds. With such a wide range of possibilities, inorganic chemistry has many facets. A widely active research area is the development and testing of transition metal complexes for catalytic, photo-physical, biochemical or manufacturing uses.

1.2 Photochemistry & Catalysis

A report of the first synthesized organometallic complex was published by Zeise in 1831.¹ To form what is now known as Zeise's salt, $\text{K}[\text{PtCl}_3(\text{C}_2\text{H}_4)] \cdot \text{H}_2\text{O}$, he mixed platinum chloride with ethanol, followed by a reaction with potassium chloride.² After some controversy to the composition of this, it was confirmed by Griess and Martius,³ and later expanded upon by Birnbaum.⁴

The field of organometallics was expanded greatly by Frankland,² and many of his complexes were catalytically active. Further development of this new type of chemistry quickly led to useful catalysts for the conversion of petroleum products or the production or destruction of other chemicals to be developed using nearly all of the transition metals. These catalysts take all forms, from simple olefin and halide compounds to multi-metallic complexes with large organic ligands.

Some of the most interesting organometallic catalysts since the late 1990s have been the development of earth metal pincer complexes to replace noble metal or early transition metal catalysts, which are often more toxic or expensive to produce. Brookhart and Gibson published a series of papers⁵⁻⁸ on the use of iron and cobalt with bis(imino)pyridine ligands to perform ethylene polymerization at rates exceeding those of similar noble metal complexes and metallocenes.⁹ The role of the ligand in the mechanism is still up for debate, but many modified systems have been synthesized and tested since the first work was published.¹⁰

Many of these types of pincer complexes are photochemically active. In transition metal complexes, the interaction between the metal atom(s) and the ligands can cause significant electron mobility upon the absorption of incident photons. The metal atom's d orbitals typically lie at or near the Highest Occupied Molecular Orbital (HOMO) energy, while the ligands often have low energy anti-bonding orbitals (π^*) at the Lowest Unoc-

cupied Molecular Orbital (LUMO) levels. When a photon is absorbed and is promoted from the ground state to the excited state, that state is geographically removed from the metal centre, this motion of the electron is labelled a Metal-Ligand Charge Transfer (MLCT). Formally, the metal atom is oxidized by the photons, this oxidation allows for redox reactivity at the metal centre for as long as the electron remains removed to the ligand. Relaxation (through photon emission via fluorescence or phosphorescence, or via vibrational or other motion processes) can return the electron to the metal to reform the ground electronic state.

1.3 Rhenium

Rewrite to
more verbose

Rhenium compounds display a broad scope of applications ranging from catalysis^{11–13} to radiopharmaceutical applications,^{14,15} as well as possessing interesting fundamental photophysical properties.¹⁶ Since the mid-1970's, complexes containing the α -diimine Re^{I} tricarbonyl core have attracted a great deal of attention due to their attractive photochemical properties with pseudo-octahedral *fac*- $[\text{L}_2\text{Re}(\text{CO})_3\text{X}]$ and *fac*- $[\text{L}_2(\text{L}')\text{Re}(\text{CO})_3]^+$ complexes being the dominant species.^{17–27} A large family of compounds with these formulations have been accessed by the addition of chelating diimine σ -donor ligands to $[\text{Re}(\text{CO})_5\text{X}]$ with the quantitative replacement of two *cis* carbonyls in the Re^{I} starting material.^{17,28–35} Significantly, these reactions form only bidentate coordinated ligands with *facial* tricarbonyl isomers as products even when a potentially tridentate σ -donor, such as bis(imino)pyridine or 2,2':6',2''-terpyridine are employed in the reaction (Figure 1.1).^{36–38} These robust species have been examined for potential applications in organic light-emitting diodes (OLEDs),³⁹ chemosensors and biotechnology probes,^{40–44} fluorescence microscopy imaging of cells,^{40,45,46} and the photochemical reduction of CO_2 to CO .^{47–51} Among the key photophysical features of these α -diimine Re^{I} compounds is the

electron transfer capability of this system and the interplay between the Re center and the well-known non-innocent redox-activity of the ligands.⁵²

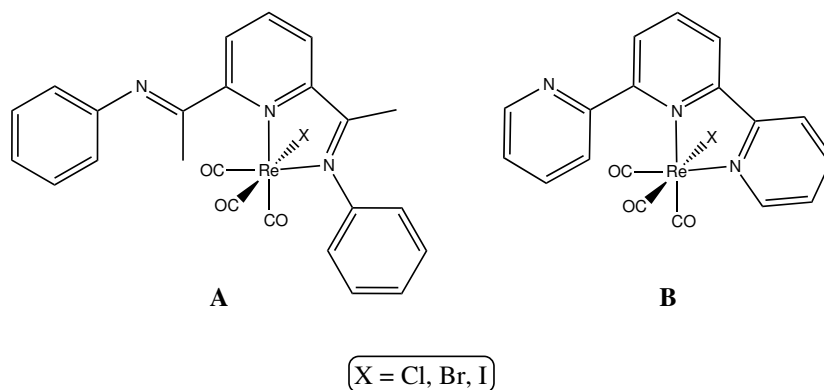


Figure 1.1 Two common *fac*-[L₂Re(CO)₃X] complexes with tridentate σ -donor ligands: L = bis(imino)pyridine (**A**) and 2,2':6',2''-terpyridine (**B**)

Further development of this chemistry has been restricted by the limited structural and electronic variability of the common pseudo-octahedral *fac*-[L₂ReX(CO)₃] (L₂ = α -diimine) products. While these systems continue to receive considerable attention, studies detailing the coordination chemistry of the meridionally-coordinated tridentate triimine Re^I dicarbonyl core are quite limited.⁵³ For example, while $\kappa^3(\text{terpy})\text{Re}(\text{CO})_2\text{Cl}$ was initially reported in 1988,⁵⁴ closer analysis of the reported analytical data (including ¹H NMR) indicate that this compound is more likely $\kappa^2\text{LRe}(\text{CO})_3\text{Cl}$. A more recent report for this compound provides spectroscopic details of this species as well as the preliminary report for the generation of [$\kappa^3(\text{terpy})\text{Re}(\text{CO})_2\text{L}$]⁺ cations (L = PPh₃, PEt₃, NC₅H₅, and NCCH₃).⁵⁵ Finally, the ¹H NMR data for $\kappa^3(\text{terpy})\text{Re}(\text{CO})_2\text{Br}$ has been reported.³⁸

In order to fully exploit the potential of this versatile family of compounds, the limits imposed by the bidentate coordination need to be addressed. Furthermore, it would appear that, on the basis of the tridentate ligands that have been investigated, the

concerted effort to produce the tridentate species has been unsuccessful. Attracted by this challenge we sought to synthesize, crystallographically authenticate, and investigate the photophysical properties of low-valent rhenium pincer complexes displaying an N,N',N''-chelated terpyridine array.

Take out
spoilers

We recently reported the conversion of bidentate bis(imino)pyridine complexes 2,6-{2,6-Me₂C₆H₃N=CPh}₂(NC₅H₃)Re(CO)₃X (X = Cl, Br) into tridentate pincer ligand compounds, 2,6-{2,6-Me₂C₆H₃N=CPh}₂(NC₅H₃)Re(CO)₂X (X = Cl, Br).⁵³ This transformation was performed in the solid-state by controlled heating of these bidentate species above 200°C in a tube furnace under a flow of nitrogen gas giving excellent yields ($\geq 95\%$). These compounds defined a new coordination environment for Re^I carbonyl chemistry where the metal center is supported by a planar, tridentate pincer coordinated bis(imino)pyridine ligand.

Complexes of 2,2':6',2''-terpyridine (terpy) are of interest due to the conceptual relationship to established bis(imino)pyridine compounds.^{56,57} Herein, we provide rational synthetic procedures to these novel species as well as their characterization and analysis of their visible electronic transitions. These results will broaden the accessibility of such compounds for investigation and application. This report for the unconventional but accessible synthesis of tridentate pincer complexes promises to enhance the versatile chemistry of Re^I and yield new venues for exploration.

This thesis will be a discussion of the development of chemistry of Re^I complexes, their characterization, and comparison of structural and photo-physical properties to computed values. Further exploration of the CO₂ reduction by photo-catalysis of these new complexes will be analyzed. This thesis will also take a more detailed look at specifics of the mechanisms proposed for current Re^I diimine catalysts, and propose new geometries for prior mechanistic steps based on experimental, computational, and

literature review work.

Chapter 2

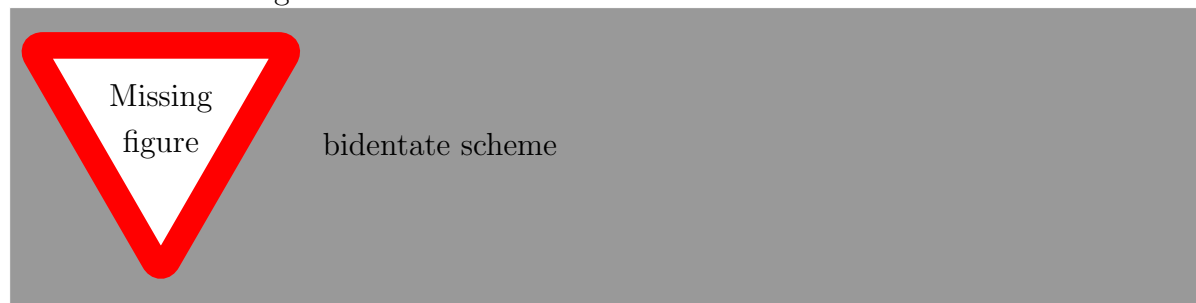
New Coordination Geometries for Re^{I}

2.1 Introduction

As mentioned previously in the thesis introduction, Re^{I} compounds have been typically bidentate (κ^2) compounds, even when using a potentially terdentate (κ^3) ligand such as bis(imino)pyridine or terpyridine (refer to Figure 1.1). The chemistry of this rhenium α -imino complex has been extensively investigated, with over 1700 references appearing in a structure search for that metal-ligand motif. The extraction of an additional carbonyl and the chelation of the pendant arm of the ligand was attempted to extend the pi system of the ligand and its interaction with the metal centre. This was first demonstrated by prior work in our group for the bis(imino)pyridine ligand.⁵³

2.2 Synthesis of Bidentate and Terdentate Re^{I} Complexes

Similar to the prior work, synthesis began with the production of the bidentate complex $\kappa^2(\text{terpy})\text{Re}(\text{CO})_3\text{X}$ ($\text{X} = \text{Cl}, \text{Br}$) by coordination of 2,2':6',2''-terpyridine (Sigma) with a $\text{Re}(\text{CO})_5\text{X}$ (Strem) starting material in dry toluene at reflux for 4 hours, as shown in Scheme 2.1. A bright yellow powder precipitated from solution and was collected by filtration, washed with cold hexanes, and dried *in vacuo* to a good yield of **1** and **3** respectively.ⁱ These bidentate compounds were characterized fully and used without further purification to produce $\kappa^3(\text{terpy})\text{Re}(\text{CO})_2\text{X}$ ($\text{X} = \text{Cl}, \text{Br}$) via thermolysis, as well as for anion exchange reactions.



Scheme 2.1 Synthesis of **1** and **2**

Conversion of compounds **1** and **3** to the κ^3 moiety required the release of CO and the subsequent coordination of the free pendant arm. Prior work had identified the thermal lability of the carbonyl, based on a method first described by Buckingham with osmium complexes.⁵⁸ In this method, a ceramic sample boat was placed in a tube furnace at elevated temperature, under a flowing atmosphere of N_2 . After some time, the sample

ⁱExperimental details for all compounds can be seen in Appendix A Experimental Procedures

is removed and collected at nearly quantitative yield. Determination of the appropriate thermolysis temperature was performed by Thermogravimetric Analysis (TGA) of the sample. A 6-8 % mass loss (dependant on sample) indicated the departure of one carbonyl group from the complex. Results of TGA on **1** and **3** is shown in Figure 2.1. For **1**, thermolysis was performed at 240°C, and for **3** thermolysis was performed at 260°C, yielding **2** and **4** respectively, at quantitative yields.

Thermogravimetric Analysis of $k^2Re(CO)_3X$

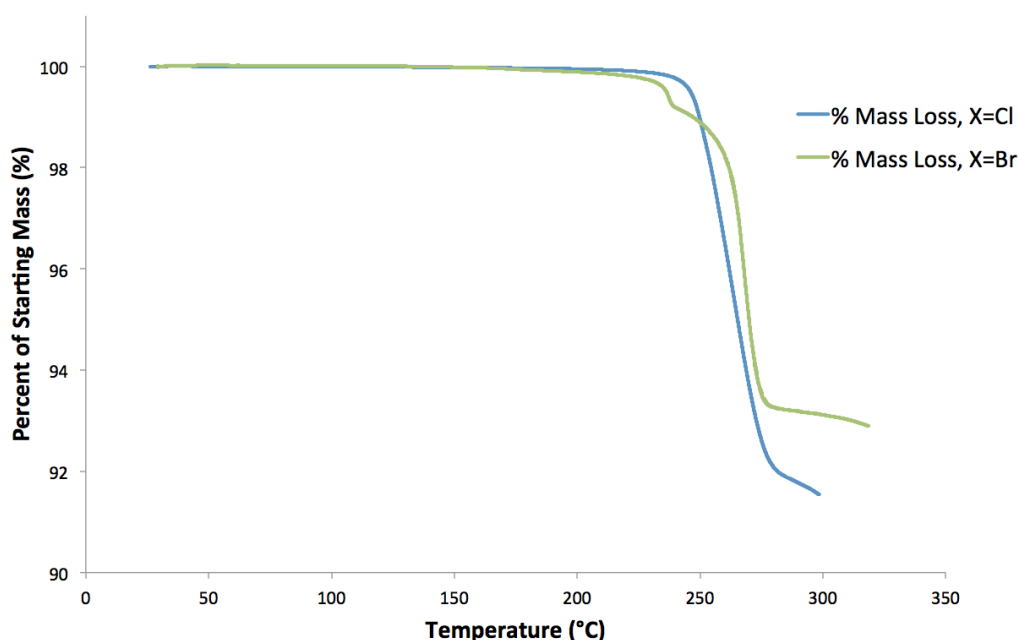
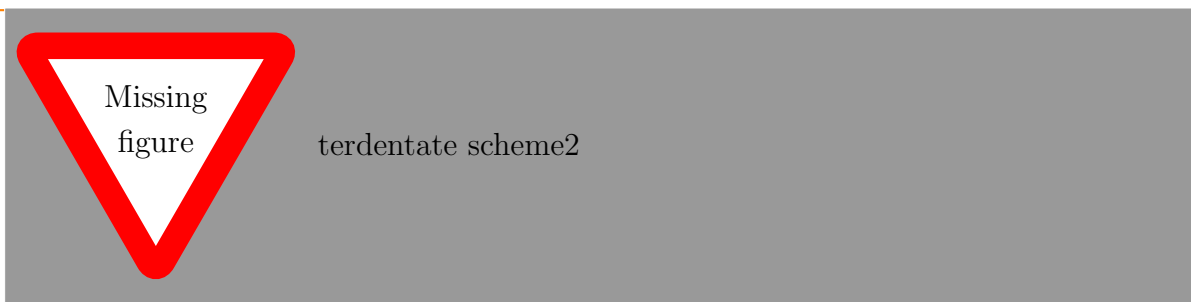
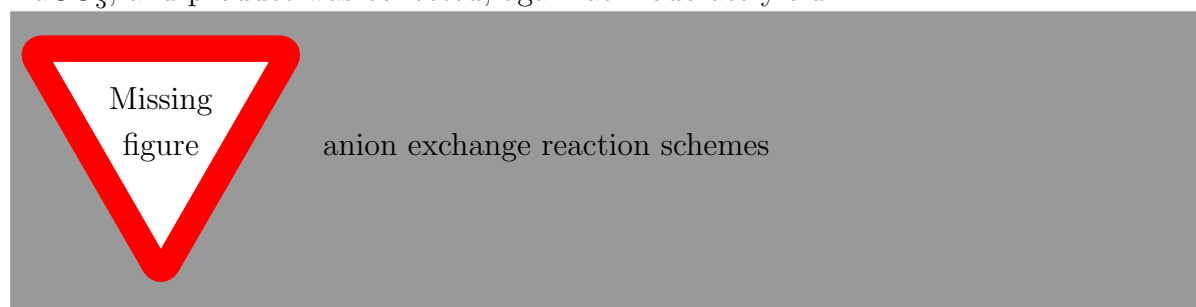


Figure 2.1 Results of TGA analysis on **1** and **3**

Further discuss TGA & terdentate rxn to build a space to put in scheme2

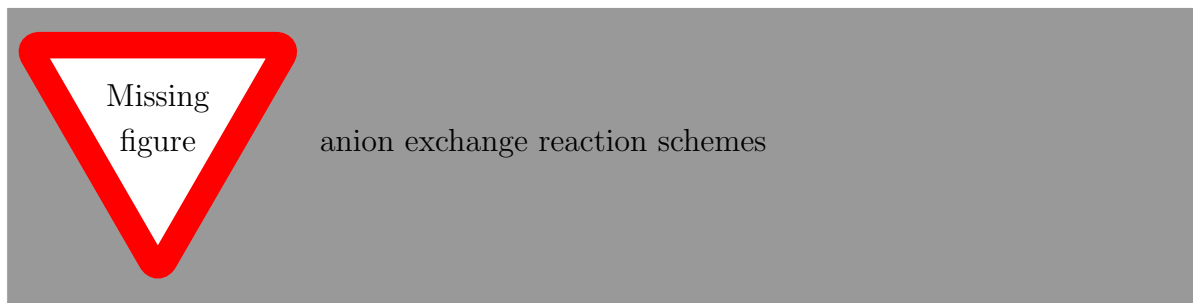


Further reactions were carried out on the above products to yield triflate and cyano complexes of bidentate and terdentate geometries. These anion exchange reactions were performed by the addition of the silver salt to **1** or **2**, to precipitate AgCl, leaving $\kappa^2(\text{terpy})\text{Re}(\text{CO})_3\text{CN}$ (**5**), $\kappa^3(\text{terpy})\text{Re}(\text{CO})_2\text{CN}$ (**6**), $\kappa^2(\text{terpy})\text{Re}(\text{CO})_3\text{OTf}$ (**7a**) and $\kappa^3(\text{terpy})\text{Re}(\text{CO})_2\text{OTf}$ (**8a**), as shown in Scheme 2.2. Resulting in only moderate yields, **7b** and **8b** were synthesized by the direct addition of neat triflic acid ($\text{CF}_3\text{SO}_3\text{H}$) to **1** and **2** respectively. HCl was released, the solutions were quenched by addition of aqueous NaCO_3 , and product was collected, again at moderate yield.



Scheme 2.2 Anion exchange pathways to synthesize **3** - **88**

A pseudo-tridentate complex was targeted to compare CO_2 photoreduction performance with the previously prepared catalysts. Typical $[\text{L}_2\text{L}'\text{Re}(\text{CO})_n]^+$ ($n = 2, 3$) targets exchange the halide for a neutral phosphine or imine type ligand, resulting in a cationic species with weakly coordinated anion (typically BF_4^- , OTf^- , BArF^- or other anion). Instead, we targeted the $\text{L}_2\text{L}'\text{Re}(\text{CO})_2\text{Cl}$ ($\text{L} = \text{bipy}$, $\text{L}' = 4\text{-}t\text{-butylpyridine}$) compound (**9**) via two similar methods (Scheme 2.3).



Scheme 2.3 Synthesis of $\text{L}_2\text{L}'\text{Re}(\text{CO})_2\text{Cl}$ ($\text{L} = \text{bipy}$, $\text{L}' = 4\text{-}t\text{-butylpyridine}$) (**9**)

2.3 Characterization

Characterization was performed on each of the products synthesized as discussed above. Nuclear Magnetic Resonance (NMR) analysis, x-ray crystallography, as well as UV-Vis and IR spectroscopy was performed. Computational Density Functional Theorem (DFT) methods were used to solve the geometries, and Time Dependant Density Functional Theorem (TD-DFT) was performed to predict UV-Vis spectra and identify electronic transitions.

2.3.1 NMR Analysis

Proton NMR was performed on each of the samples. Each sample was dissolved completely in deuteroacetonitrile (CD_3CN) and analysis was performed on a Bruker AVANCE 400 MHz spectrometer. Data was processed from the FID signal via the TopSpin program, and spectra were analyzed using ACD NMR Processor v12.0.

Detailed peak analysis comparing bidentate samples **1**, **3**, **5**, and **7** or terdentate **2**, **4**, **6**, and **8** show little difference between samples. This is due to the distance between

the anion and any protons on the ligand. While anions with different σ donor strength marginally impact the metal-ligand interactions, these have only small effect on the location of peaks, shifting between samples by typically less than 0.1 ppm. As is shown in Figure 2.2, the characteristic shape of each spectra remains constant, only exact peak locations and some peak order varies with anion choice.

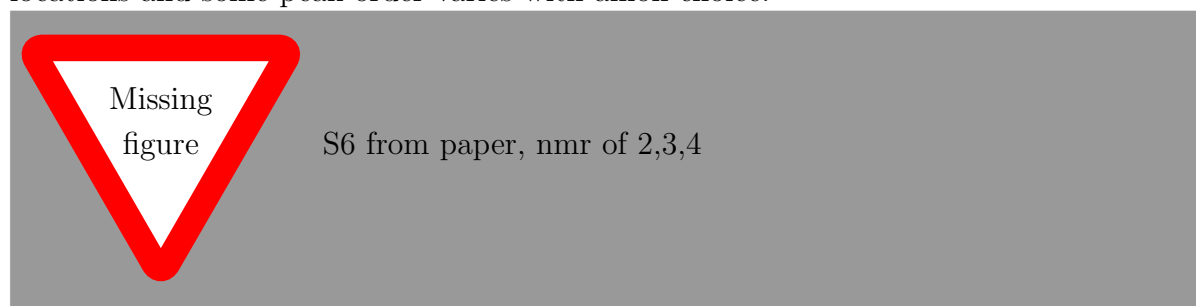
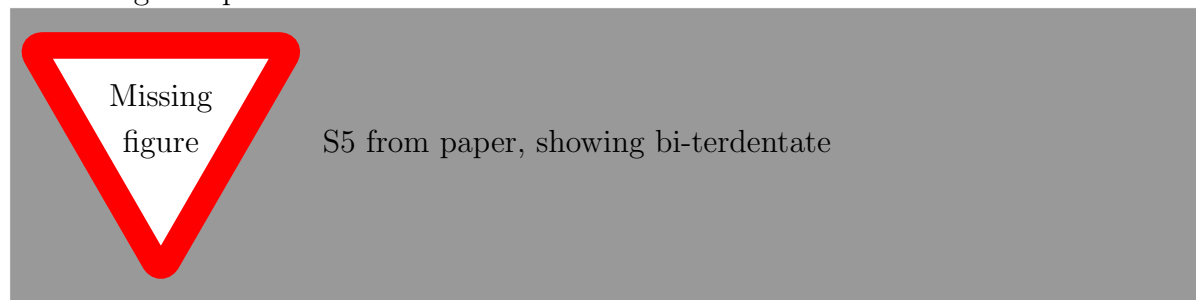


Figure 2.2 The aromatic region of the 1H NMR spectra for compounds (red), (green), and (blue)

The characteristic feature in the NMR spectra after the transformation from bidentate to terdentate (e.g. sample **1** to **2**) is the simplification of the signals in the aromatic region (between 7 and 9 ppm). This simplification is due to the increased symmetrization of the ligand, while the κ^2 bidentate ligand has a freely rotating pendant group, the κ^3 terdentate ligand is in a more rigidly fixed geometry. Prior work in literature and in our group shows the temperature dependence of the rate of rotation of this pendant arm for various ligand species.



check compounds & spectra

Get paper citation

Titel's Thesis citation

Figure 2.3 The aromatic region of the ^1H NMR spectra for compounds (red) and (blue), showing the simplification of the spectra upon the conversion from bidentate to terdentate

check compounds & spectra

Put in nmr peak values

The simplification of peaks due to the symmetrization of the ligand results in the peaks from () and () aligning with their mirror peaks at () and (). ?? shows the proton expanded ligand, the peaks at () and () correspond with the protons () and ().

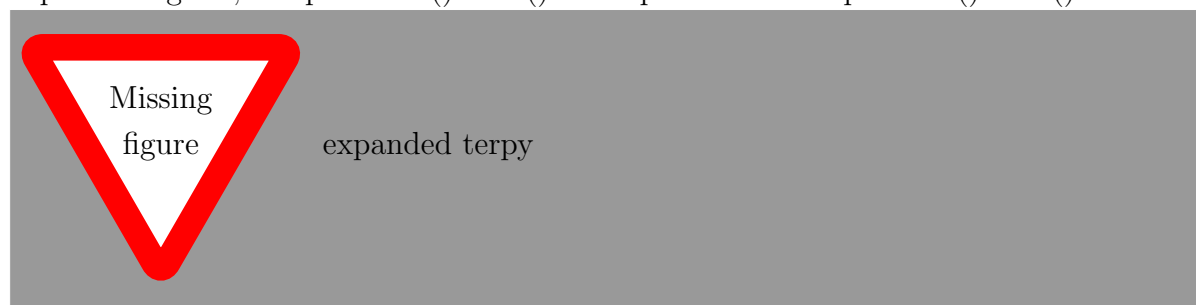


Figure 2.4 Proton-explicit skeletal drawing of 2,2':6',2''-terpyridine

Carbon NMR (^{13}C) was attempted on the complexes as well. Unfortunately, Re^{I} complexes perform poorly in ^{13}C NMR experiments, the signal to noise ratio is incredibly poor (if a signal is even visible). The effect of this is a lack of ^{13}C NMR analysis of these compounds in literature, with a very few exceptions.

why poor, show an ok result & discuss

2.3.2 X-Ray Crystallography

Single crystal analysis by x-ray crystallography yielded good structures of compounds **1**, **2**, **3**, **4**, . These are the first reported crystal structures of the κ^3 terdentate Re^{I} com-

the rest of structures

pounds. A number of structural characteristics are common between the various bidentate or terdentate complexes. Much analysis has been done on the structures of bidentate complexes in literature, the notable characteristic within terpyridine compounds is the rotation of the pendant arm pushing the nitrogen atom away from the plane of the metal-ligand bonds by approximately 100° . Cell parameters and other collection data for compounds **1**, **3**, **5**, and **7** are located in Table 2.4.

Sample **3**'s crystal structure had a higher symmetry than the other samples. Details on the exact methods used for structure elucidation are available in section A.3, but all of the structures found are of high quality. The structures of **1**, **3**, and **5** can be seen in Figure 2.5, Figure 2.6 and Figure 2.7, respectively, and more views of these structures can be seen in section A.3. Crystals suitable for x-ray analysis were unable to be collected from compound **7**.

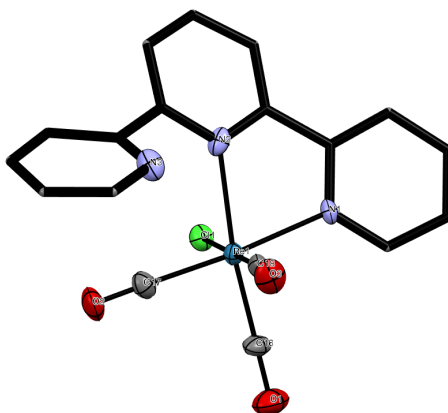


Figure 2.5 X-ray crystal structure representation for **1**. Only one of the two of the molecules in the unit cell are shown. Co-crystallized chloroform, hydrogen atoms, and thermal ellipsoids of ligand carbon atoms are omitted for clarity.

Selected bond lengths, bond angles, and torsions are listed in Table 2.1, Table 2.2 and Table 2.3 for products **1**, **3**, and **5** respectively. The structures can be seen in Figure 2.5, Figure 2.6 and Figure 2.7, and more views of these structures can be seen in Appendix A,

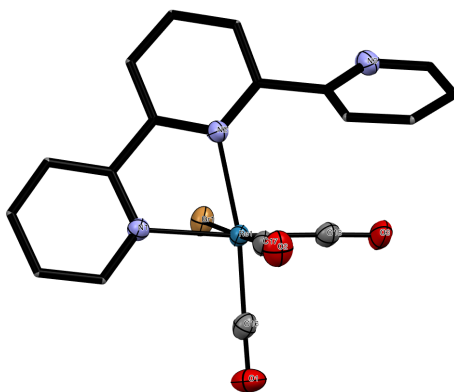


Figure 2.6 X-ray crystal structure representation for **3**. Co-crystallized chloroform, hydrogen atoms, and thermal ellipsoids of ligand carbon atoms are omitted for clarity.

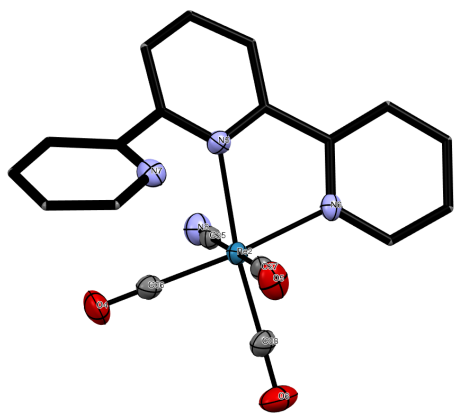


Figure 2.7 X-ray crystal structure representation for **5**. Only one of the two of the molecules in the unit cell are shown. Co-crystallized chloroform, hydrogen atoms, and thermal ellipsoids of ligand carbon atoms are omitted for clarity.

subsection A.3.1, X-Ray Structures from Multiple Vantage Points.

The Re^{I} centre in the pseudooctahedral complex is supported by a planar, pincer coordinated ligand defined by the terminal and central pyridyl group of the terpyridine. One of the carbonyl groups lies in this plane trans to the central pyridyl group, while the remaining carbonyl groups and the anionic group or other complexed species lie on an approximately perpendicular plane to the ligand. Bond angles around the Re centre show a significant deviation of up to 15° from the ideal octahedral geometry for all samples analyzed. The typical N-Re-N bond angle of 75° is due to the atomic size of rhenium, comparison to the crystal structure of an analogous compound with a manganese atom⁵⁹ shows an increase in the bonding angle by approximately 4° due to a decrease of bond length from metal to nitrogen of about 0.12 Å for both the central and terminal pyridines.

The deviation from octahedral is further visible in the rotation of the X-Re-CO plane (X=halide, anion, complexed group) by approximately 10 degrees from the right angle relative to the plane of the ligand. The axial halide, anion, or chelated group typically occupies a position such that it is slightly eclipsing the ligand, when viewed from the axial position. This eclipsing is due to some unknown process, no steric interference exists upon that site, analysis of electrostatic or other short-range electronic effects show any interaction between this site and the aromatic rings. In Re^{I} complexes, the halide or anion is located axial relative to the plane of the ligand. For the acetonitrile complex with triflate counterion, the acetonitrile occupies the axial position. This site occupation holds through the complete set of x-ray crystal structures with a $\kappa^2\text{-(bipy)Re(CO)}_3\text{X}$ core structure motif deposited in the Cambridge Crystallography Data Centre (CCDC) database,⁶⁰ and extends through other α -diimine complexes seen in our lab and in literature.⁵³

The crystal structure for compound **5** contains two molecules per unit cell, one of

which is solved to have the cyano group in the position trans to the ligand. However, careful analysis of the bond lengths, angles, and torsion data in Table 2.3 shows a remarked similarity between all -CO and -CN groups. Additionally, in an x-ray diffraction pattern, -CN and -CO look quite similar. Thus, while the structure solved to the two isomers, critical analysis would suggest that this molecule does not violate the axial position pattern laid out above.

Selected bond lengths, bond angles, and torsions are listed in Table 2.1, Table 2.2 and Table 2.3 for products **1**, **3**, and **5** respectively.

Structural comparisons between the bidentate samples and the terdentate show many similarities. The loss of one carbonyl always accompanies the dentation of the pendant arm of the ligand. The increased coordination forces the ligand to adopt a more rigidly planar geometry, this is visible in the structure of **2** (Figure 2.8) and **8** (Figure 2.9). Structures for other discusses species were unable to be collected.

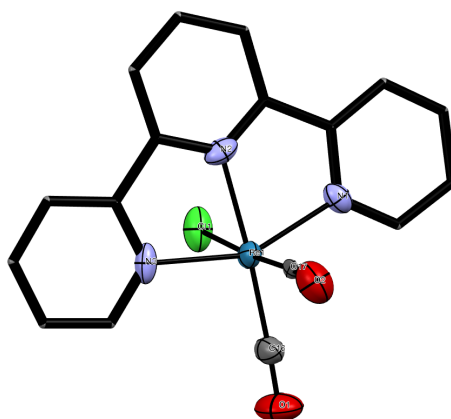


Figure 2.8 X-ray crystal structure representation for **1**. Only one of the two of the molecules in the unit cell are shown. Co-crystallized chloroform, hydrogen atoms, and thermal ellipsoids of ligand carbon atoms are omitted for clarity.

Selected bond lengths, bond angles, and torsions are listed in ?? and ?? for products

not done

2 and **8**. Cell parameters and collection data can be found in Table 2.5.

Table 2.1 Selected Distances, Angles, and Torsions for **1**

Selected Distances (Å)	
Re(1)-C(16)	1.89(1)
Re(1)-C(17)	1.934(8)
Re(1)-C(18)	1.90(1)
Re(1)-N(1)	2.162(6)
Re(1)-N(2)	2.236(9)
Re(1)-Cl(1)	2.496(2)
Selected Angles (deg)	
C(16)-Re(1)-C(17)	87.6(4)
C(16)-Re(1)-C(18)	88.3(4)
C(17)-Re(1)-C(18)	87.3(4)
C(16)-Re(1)-N(1)	96.4(3)
C(17)-Re(1)-N(1)	174.9(3)
C(18)-Re(1)-N(1)	95.9(3)
C(16)-Re(1)-N(2)	169.3(3)
C(17)-Re(1)-N(2)	101.1(3)
C(18)-Re(1)-N(2)	98.3(3)
N(2)-Re(1)-N(1)	74.5(3)
C(16)-Re(1)-Cl(1)	91.7(3)
C(17)-Re(1)-Cl(1)	91.7(3)
C(18)-Re(1)-Cl(1)	179.9(3)
N(1)-Re(1)-Cl(1)	84.0(2)
N(2)-Re(1)-Cl(1)	81.6(2)
O(1)-C(16)-Re(1)	179.6(9)
O(2)-C(17)-Re(1)	176.0(8)
O(3)-C(18)-Re(1)	177.3(9)
Selected Torsions (deg)	
N(1)-C(5)-C(6)-N(2)	16(1)
N(2)-C(10)-C(11)-N(3)	41(1)

Table 2.2 Selected Distances, Angles, and Torsions for **3**

Selected Distances (Å)	
Re(1)-C(16)	1.911(3)
Re(1)-C(17)	1.890(3)
Re(1)-C(18)	1.921(4)
Re(1)-N(1)	2.173(3)
Re(1)-N(2)	2.232(2)
Re(1)-Br(1)	2.6410(4)
Selected Angles (deg)	
C(16)-Re(1)-C(17)	89.1(1)
C(16)-Re(1)-C(18)	85.9(1)
C(16)-Re(1)-N(1)	97.9(1)
C(17)-Re(1)-N(1)	92.5(1)
C(18)-Re(1)-N(1)	175.4(1)
C(16)-Re(1)-N(2)	171.2(1)
C(17)-Re(1)-N(2)	96.0(1)
C(18)-Re(1)-N(2)	101.3(1)
N(1)-Re(1)-N(2)	74.7(1)
C(16)-Re(1)-Br(1)	92.7(1)
C(17)-Re(1)-Br(1)	177.6(1)
C(18)-Re(1)-Br(1)	91.6(1)
N(1)-Re(1)-Br(1)	85.74(7)
N(2)-Re(1)-Br(1)	82.07(7)
O(1)-C(16)-Re(1)	178.6(3)
O(2)-C(17)-Re(1)	179.5(3)
O(3)-C(18)-Re(1)	179.9(3)
Selected Torsions (deg)	
N(1)-C(6)-C(1)-N(2)	-15.4(4)
N(2)-C(5)-C(11)-N(3)	141.1(3)

Table 2.3 Selected Distances, Angles, and Torsions for **5**

Selected Distances (Å)			
Cyanide Axial		Cyanide Trans	
Re(2)-C(35)	2.148(7)	Re(1)-C(19)	2.105(8)
Re(2)-C(36)	1.926(6)	Re(1)-C(16)	1.928(5)
Re(2)-C(37)	1.954(7)	Re(1)-C(18)	1.96(1)
Re(2)-C(38)	1.902(9)	Re(1)-C(17)	1.918(7)
Re(2)-N(5)	2.242(7)	Re(1)-N(1)	2.253(5)
Re(2)-N(6)	2.168(5)	Re(1)-N(2)	2.176(4)
C(35)-N(8)	1.138(9)	C(19)-O(3)	1.17(1)
C(36)-O(4)	1.145(8)	C(16)-N(4)	1.149(7)
C(37)-O(5)	1.151(9)	C(18)-O(2)	1.14(1)
C(38)-O(6)	1.17(1)	C(17)-O(1)	1.130(8)
Selected Angles (deg)			
Cyanide Axial		Cyanide Trans	
C(16)-Re(1)-C(17)	87.8(3)	C(36)-Re(2)-C(38)	87.7(3)
C(16)-Re(1)-C(18)	87.0(3)	C(36)-Re(2)-C(37)	88.0(3)
C(16)-Re(1)-C(19)	92.5(3)	C(36)-Re(2)-C(35)	92.1(3)
C(17)-Re(1)-C(18)	88.7(3)	C(38)-Re(2)-C(37)	88.5(3)
C(17)-Re(1)-C(19)	90.5(3)	C(38)-Re(2)-C(35)	90.8(3)
C(18)-Re(1)-C(19)	179.1(3)	C(37)-Re(2)-C(35)	179.2(3)
C(16)-Re(1)-N(1)	102.2(2)	C(36)-Re(2)-N(5)	100.6(3)
C(16)-Re(1)-N(2)	175.9(2)	C(36)-Re(2)-N(6)	174.2(3)
C(17)-Re(1)-N(1)	168.3(3)	C(38)-Re(2)-N(5)	169.3(3)
C(17)-Re(1)-N(2)	95.9(3)	C(38)-Re(2)-N(6)	96.6(3)
C(18)-Re(1)-N(1)	97.7(3)	C(37)-Re(2)-N(5)	98.4(2)
C(18)-Re(1)-N(2)	94.8(3)	C(37)-Re(2)-N(6)	96.0(2)
C(19)-Re(1)-N(1)	83.2(2)	C(35)-Re(2)-N(5)	82.3(2)
C(19)-Re(1)-N(2)	85.7(2)	C(35)-Re(2)-N(6)	83.9(2)
N(1)-Re(1)-N(2)	73.9(2)	N(5)-Re(2)-N(6)	74.7(2)
O(1)-C(17)-Re(1)	178.2(7)	O(6)-C(38)-Re(2)	179.4(7)
O(2)-C(18)-Re(1)	172.0(7)	O(5)-C(37)-Re(2)	175.5(6)
O(3)-C(19)-Re(1)	178.0(6)	N(8)-C(35)-Re(2)	178.0(6)
N(4)-C(16)-Re(1)	178.7(6)	O(4)-C(36)-Re(2)	179.0(7)
Selected Torsions (deg)			
Cyanide Axial		Cyanide Trans	
N(1)-C(1)-C(6)-N(2)	12.5(8)	N(5)-C(20)-C(25)-N(6)	14.5(9)
N(1)-C(5)-C(11)-N(3)	43.7(9)	N(5)-C(24)-C(30)-N(7)	41(1)

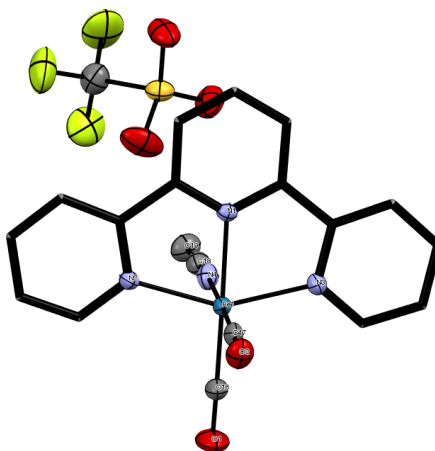


Figure 2.9 X-ray crystal structure representation for **3**. Co-crystallized chloroform, hydrogen atoms, and thermal ellipsoids of ligand carbon atoms are omitted for clarity.


Table 2.4 Crystal data and structure refinement for compounds **1**, **3**, **5**, and **7**

Compound	1	3	5	7
Empirical formula	$\text{C}_{19}\text{H}_{11}\text{N}_3\text{O}_3\text{ReCl}$	$\text{C}_{19}\text{H}_{11}\text{N}_3\text{O}_3\text{ReBr}$	$\text{C}_{20}\text{H}_{11}\text{N}_4\text{O}_3\text{Re}$	$\text{C}_{22}\text{H}_{14}\text{N}_4\text{O}_6\text{F}_3\text{SRe}$
Formula weight (g/mol)	538.96	583.41	530.04	693.63
Temperature (K)	200(2)	200	200	200
Wavelength (\AA)	0.71073	0.71073	0.71073	0.71073
Crystal System	Triclinic	Monoclinic	Triclinic	
Space Group	P-1	C2/c	P-1	
a (\AA)	9.8736(4)	31.1537(7)	9.9196(9)	
b (\AA)	14.8202(4)	7.1176(2)	14.9902(14)	
c (\AA)	16.3472(4)	16.8519(4)	16.5187(15)	
α (deg)	69.2890(10)	90.000	68.363(2)	
β (deg)	80.801(2)	111.0230(10)	80.929(2)	
γ (deg)	79.836(2)	90.000	79.975(2)	
Volume (\AA^3)	2190.00(12)	3488.00	2236.6(4)	
Z, r (calc) (Mg/m^3)	2, 1.997	8, 2.222	2, 1.927	
Absorption coefficient (mm^{-1})	6.063	9.282	5.821	
Absorption correction		Semi-empirical from equivalents		
Final R indices [$I \geq 2\sigma(I)$]	R1 = 0.0397, wR2 = 0.0839	R1 = 0.0232, wR2 = 0.0614	R1 = 0.0390, wR2 = 0.0921	
R indices (all data)	R1 = 0.0604, wR2 = 0.0951	R1 = 0.0285, wR2 = 0.0642	R1 = 0.0500, wR2 = 0.0961	

Table 2.5 Crystal data and structure refinement for compounds **2**, **4**, **6**, and **8**

Compound	2	4	6	8
Empirical formula	$\text{C}_{18}\text{H}_{11}\text{N}_3\text{O}_2\text{ReCl}$	$\text{C}_{18}\text{H}_{11}\text{N}_3\text{O}_2\text{ReBr}$	$\text{C}_{19}\text{H}_{11}\text{N}_4\text{O}_2\text{Re}$	$\text{C}_{21}\text{H}_{14}\text{N}_4\text{O}_5\text{F}_3\text{SRe}$
Formula weight (g/mol)	510.95	530.04	502.04	665.61
Temperature (K)	200(2)	200	200	200
Wavelength (Å)	0.71073	0.71073	0.71073	0.71073
Crystal System	Triclinic			Triclinic
Space Group	P-1			P-1
a (Å)	8.5275(3)			8.5745(4)
b (Å)	14.2421(5)			11.9805(5)
c (Å)	17.4637(6)			13.0970(5)
α (deg)	77.948(2)			79.748(2)
β (deg)	85.684(2)			81.106(2)
γ (deg)	79.890			88.091(2)
Volume (Å ³)	2041.79(12)			1307.99(10)
Z, r (calc) (Mg/m ³)	4, 2.050			2, 1.993
Absorption coefficient (mm ⁻¹)	6.494			5.094
Absorption correction		Semi-empirical from equivalents		
Final R indices [$I \geq 2\sigma(I)$]	R1 = 0.0636, wR2 = 0.1018			R1 = 0.0294, wR2 = 0.0673
R indices (all data)	R1 = 0.0985, wR2 = 0.1110			R1 = 0.0366, wR2 = 0.0700

2.3.3 Infrared Spectroscopy

Conversion of bidentate to terdentate species was confirmed utilizing Fourier Transform Infrared (FTIR) spectroscopy. A small sample of powder product was placed on a  instrument, with and for a .

Analysis of the results shows the loss of one peak in the (ca.) 2000 cm^{-1} region. This peak is in the CO stretching frequency, the frequency of the peak lost in thermolysis is indicative of a weakly coordinated carbonyl group. A shift occurs for one peak in the conversion from bidentate to terdentate, from 1890 to 1790 cm^{-1} , indicating the further weakening of the metal carbonyl bonds remaining in the complex. This weakened bond is likely the carbonyl co-planar to the ligand, analysis of the x-ray crystal structure shows the CO bond to be 0.1 \AA longer than that of the axial carbonyl. Further analysis of the spectra were not successful in identification of any additional molecular properties, with the exception of a series of strong peaks appearing in the $1200\text{--}1300\text{ cm}^{-1}$ range, confirming the presence of the triflate anion from the $-\text{SO}_3$ group vibrations.

2.3.4 Photophysical Properties

A striking observation upon the conversion of the bidentate species into the terdentate complexes is that these new compounds have a substantially darker colour that reflects a significant change in the photophysical properties. This effect was investigated using a combination of UV-visible spectroscopy and DFT modelling. The stronger absorbance of the terdentate complexes compared to the bidentate precursors is evident in the UV-Vis spectra of these species, and is presented in Figure 2.13. These spectra were obtained in Dimethylsulfoxide (DMSO) with approximate concentrations of 0.01 mM for bidentate, and an order of magnitude lower (0.001 mM) for the terdentate analogues. The tridentate complexes have more intense absorbance for higher energy ligand UV-based $\pi\text{--}\pi^*$

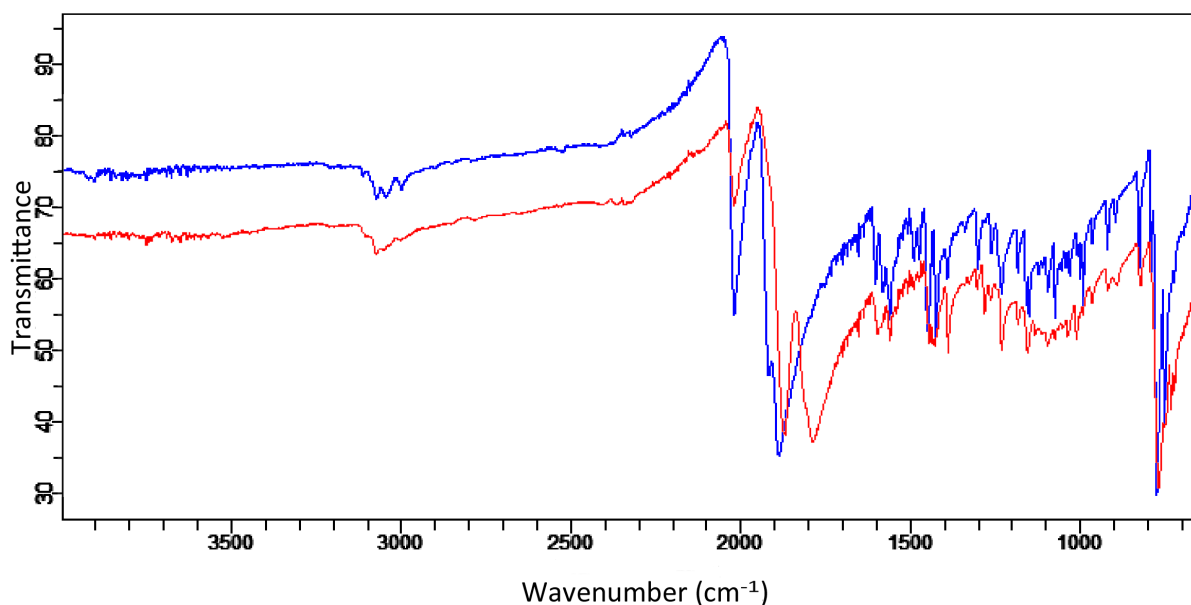
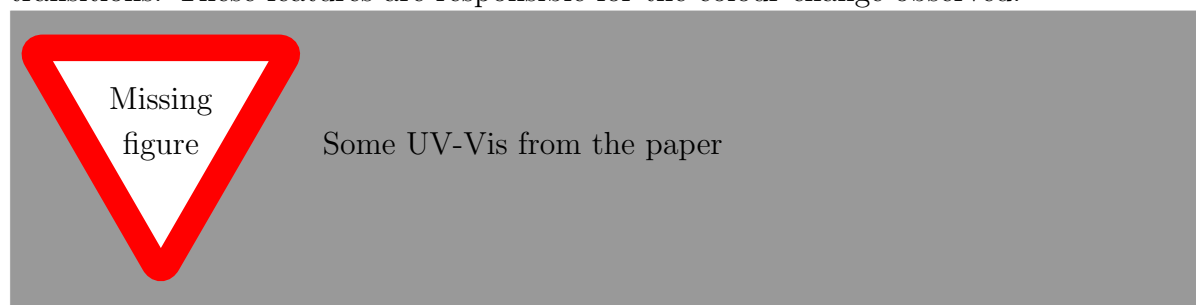


Figure 2.10 FTIR Spectra for complexes **1** (blue) and **2** (red).

transitions ($\leq 400nm$) and certainly a rich visible absorption profile that involves π^* transitions. These features are responsible for the colour change observed.



More UVVIS discussion.

This will be longer. Should be lots of discussion about results differences. I need to a) highlight the importance of anion exchange, and then b) highlight the importance of bidentate vs. terdentate

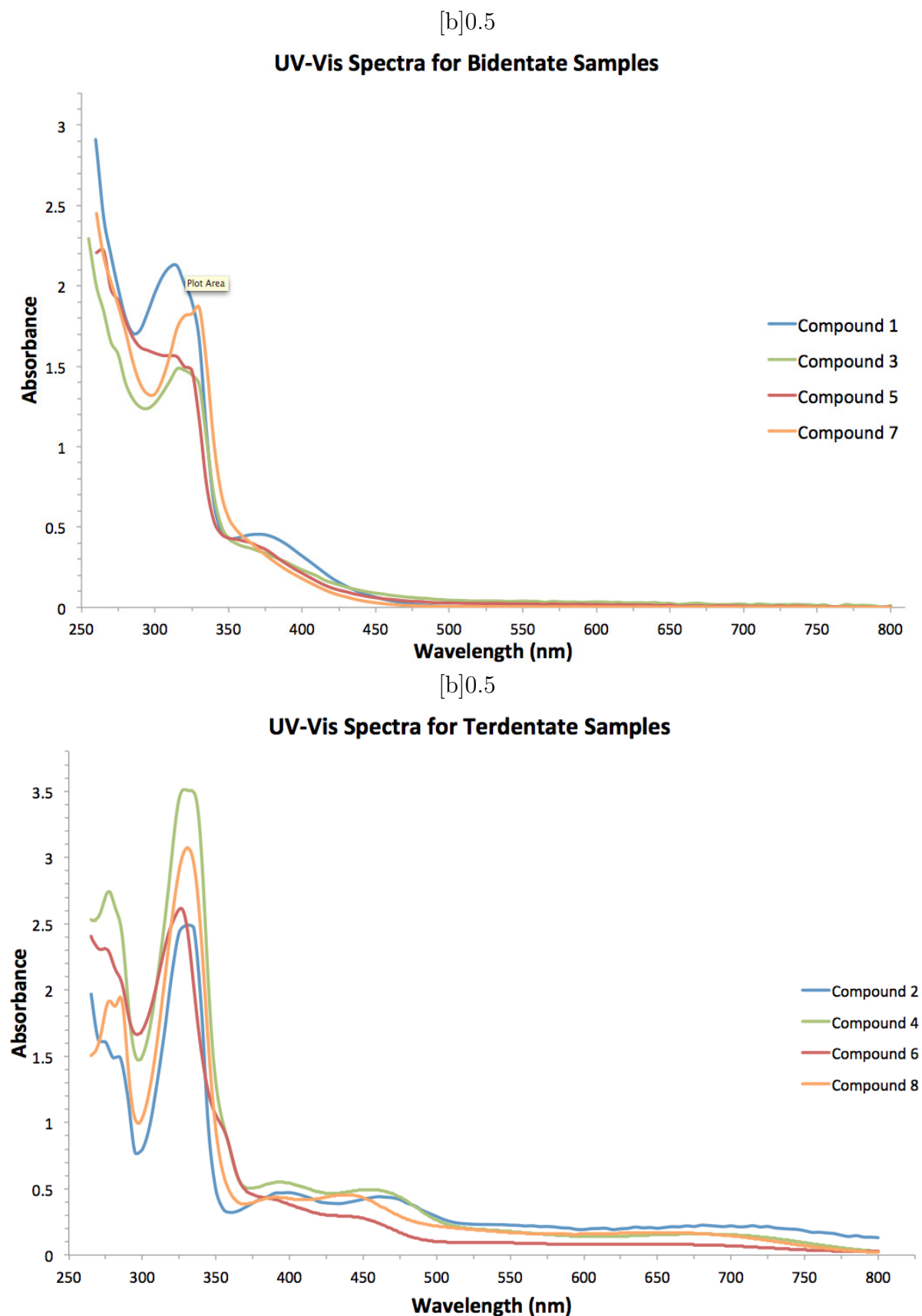


Figure 2.13 UV-Vis spectra for all compounds. Concentrations of bidentate complexes are 0.01 mM and terdentate complexes are 0.001 mM.

UV-Vis Spectroscopy

This will be longer. Should be lots of discussion about results differences. I need to
a) highlight the importance of anion exchange, and then b) highlight the importance
of bidentate vs. terdentate

2.4 Conclusions

Conclusion shows that manipulations can be done, this affects the photophysical
properties of the compounds and may affect the photochemical

Chapter 3

Photocatalysis of CO₂

3.1 Introduction

Only 6 years after Re^I complexes using 2,2'-bipyridine were characterized, Hawecker, Ziessel, and Lehn showed the effectiveness of the compound for the catalytic photoreduction of CO₂.⁴⁷ Since then, many have shown the efficacy of a wide range of α -diimino complexes for the reaction, and expansion of the systems to dimetallic complexes with ruthenium and osmium as electron transfer agents has produced a wide range of results. The mechanism of reduction has been subject of some debate, while mechanisms have been proposed since Lehn et. al. soon after their original publication,⁴⁸ modifications have been submitted routinely over the past decades. Further discussion and a proposal of a new mechanism geometry based on computational and experimental data can be read in chapter 4.

check ref
names

a few refer-
ences

refer to these
as well. Red
Light paper?

references,
Morris, JACS
dimer, mech.
basis

3.2 Photocatalytic Reactions with New Compounds

The photocatalytic cycle is, simply, a photon-induced MLCT, followed by the extraction of an electron from a sacrificial reductant. This radical, negatively charged species sheds the anion, opening up a reaction site. Reaction between a CO₂, a proton (from the decomposition of the reductant or elsewhere), and the catalyst yields any number of CO, H₂O, formate (HCO₂⁻), or carbonate (CO₃H⁻), depending on the mechanistic pathway.

3.2.1 Conditions

Reaction conditions in use in literature have remained typically unchanged since the original papers. A mixture of N,N-dimethylformamide (DMF) with either Triethanolamine (TEOA) or Triethylamine (TEA) at a 5:1 ratio is used to make a 1.0 mM solution of catalyst, with 'excess' (a 1.1 to 25 molar ratio) electrolyte salt (typically Et₄NX or *t*-Bu₄NX, where X = halide in catalyst) added as a stabilizer. Solutions are degassed by bubbling of CO₂ and a consistent headspace is left to form over the solution. The reaction is monitored via Gas Chromatography (GC) analysis of the headspace, using a HP gas chromatograph with a 15 m CARBONPLOT column with 0.320 mm inner diameter and 1.50 μm film in a 40°C oven. The instrument is fitted with a Thermal Conductivity Detector (TCD), and, while using He as a carrier gas, is able to resolve CO and CO₂ completely.

3.2.2 Experimental Results

Both bidentate and terdentate $\kappa^n(\text{terpy})\text{Re}(\text{CO})_{5-n}\text{X}$ (n=2,3) complexes show no activity for CO₂ reduction. Modification of testing time, light source, product analysis methods, solvent, sacrificial reductant, pH, presence of electrolyte, presence of H₂O, or

variation of anion (X=Cl, Br, OTf, CN) shows no change of this inactivity. Testing of $\kappa^2(\text{bipy})\text{Re}(\text{CO})_3\text{Cl}$ under the same reaction conditions shows production of approximately 6 mL CO from CO₂ (20% conversion) in 1 hour of photolysis with visible ($\lambda > 400\text{nm}$) light.

SubSubSection

SubSubSection

SubSubSection

3.3 Section


3.4 Section

3.4.1 Subsection

Chapter 4

Mechanism of CO₂ Reduction

4.1 Introduction

Within three years of the originally reported bipyridine rhenium I catalyst, experimental studies on the mechanism of the photocatalytic reduction of CO₂ were available in the literature.⁴⁸  Studies continue on the mechanism up to the present day^{61,62}, utilizing new investigative techniques as they become available, this includes the use of DFT methods to elucidate geometries of intermediates and transition states for of the multi-step cycle. Transition metal catalysis is a non-trivial problem computationally, especially when considering a metal from the lower period. These elements contain a large amount of electrons, many of which can be involved in non-covalent interactions with the ligands and catalyzed products. Solving for this complex system becomes non-trivial and computationally expensive. For this reason, no overview of the mechanism as investigated by DFT methods has ever been made available in the literature.

4.2 Literature Mechanisms

Prior work in the literature has proposed three general mechanistic pathways for the photoreduction of CO₂. In general, as seen in Figure 4.1, these pathways result in the formation of CO and H₂O, formate (HCO₂⁻), or carbonate (CO₃H⁻) anions. The formation of carbonate proceeds via the formation of a catalyst dimer over a molecule of CO₂, with the insertion of a second molecule of CO₂ to produce the carbonate and a molecule of CO. Formation of formate occurs via insertion of CO₂ to a rhenium hydride bond. The formation of CO without carbonate or formate by-products occurs via the coordination of CO₂ to an open site on the metal, followed by a double proton addition and the release of a molecule of H₂O prior to the loss of one of the four carbonyl groups to open up the axial site for halide re-coordination. The activation of the catalyst with respect to radicalization, electron abstraction from the sacrificial reductant, and anion disassociation is well studied, the character of the CO₂ adduct is less well known.

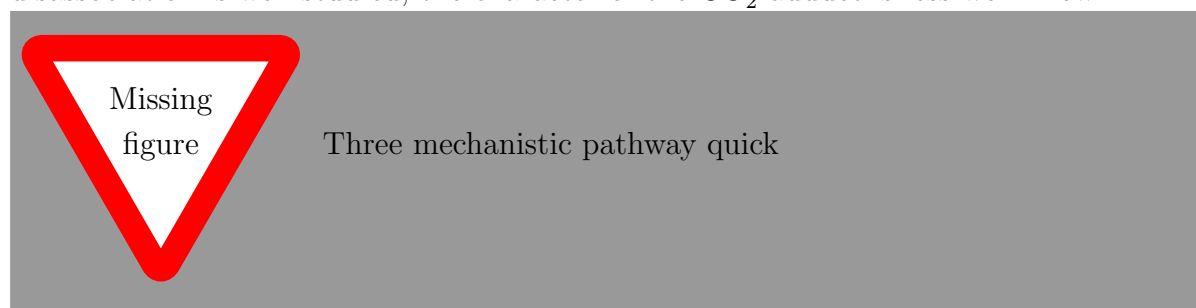


Figure 4.1 An overview of the mechanistic pathways of photochemical CO₂ reduction

Many of the intermediates have been synthesized in various studies, indicating their reasonable stability. While individual portions of the mechanism have been studied computationally in the past, no over-arching study has compared methods relative to each other. Furthermore, while the formation of CO with H₂O is the most anticipated

Make mechanism (or get morris?)

Ref. Sullivan and Gilbert

refs

pathway (due to the lack of formation of carbonate or formate in most studies), no literature pathway exists to explain the addition of CO₂ to the open site of the radical catalytic species without a three body reaction step (catalyst, CO₂ and H⁺ together) or without formate reorganization. Furthermore, no mechanism proposed thus far explains the ¹²CO to ¹³CO isotopic exchange demonstrated by Lehn's group in 1986.⁴⁸

4.3 Consequences From κ^2 Terpyridine Complex Inactivity

The lack of reactivity of the $\kappa^2(\text{terpy})\text{Re}(\text{CO})_3\text{X}$ motif of complexes contrasting to the activity of the originally published $\kappa^2(\text{bipy})\text{Re}(\text{CO})_3\text{X}$ indicates some influence of the ligand on the mechanism. While the terdentate complex can be rationalized to be inactive due to its short-lived excited state (as seen in the lack of fluorescence), this explanation does not suffice for the fluorescing bidentate complex. Other substituted bipyridine ligands are known to be active for photocatalytic reduction, identifying the most likely conflicting feature of the terpyridine ligand to be the pendant arm, and its availability for chelation to the metal centre. While in the radical eximer form, the chelation site is sterically blocked by one of the three carbonyl groups. However, reorganization of the substituent carbonyls from a *facial* orientation to a *meridional* could allow for the free pyridine to form the metal-ligand bond, resulting in compound (X).

Due to the ease of migration of the carbonyl groups, it is proposed that the mechanism that follows pathway X does not occur entirely axial to the ligand, but begins with coordination of a CO₂ molecule in between the *facial*-CO ligands, forcing a carbonyl to the axial position. This CO₂ bound in the plane of the ligand then undergoes hydrogenation to produce a molecule of H₂O. After the departure of the water molecule,

fluorescence tests on 1,2

ref lehn88?

Set up a detailed naming scheme that will work for the entire chapter, likely having to start with

the catalyst is left as a tetracarbonyl cation. While any of the carbonyl groups could be labile, the carbonyl at the axial position is replaced by the halide to return to the starting catalyst.⁶³

4.4 Comparison Between Mechanistic Pathways

The overall energies for each of the mechanistic pathways shown in Figure 4.1 are shown in Figure 4.2.

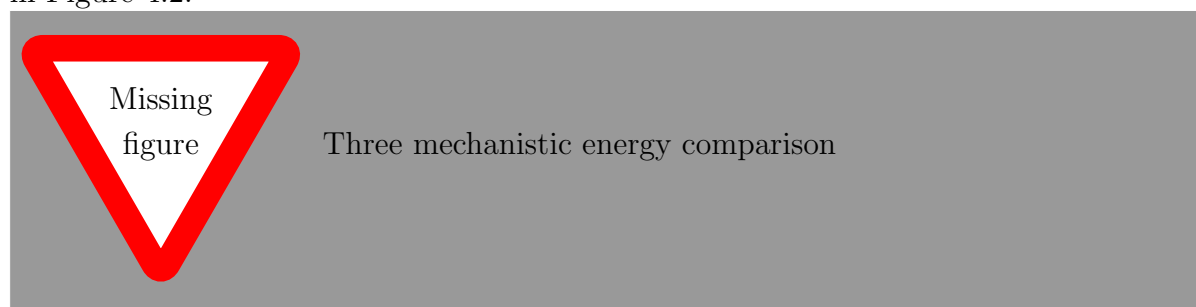


Figure 4.2 An overview of the energies of the three mechanistic pathways of photochemical CO₂ reduction

SOLVE EN-
ERGY

4.4.1 Subsection

SubSubSection

SubSubSection

SubSubSection

Chapter 5

Conclusions

The target Re^{I} terdentate terpyridine compounds were successfully synthesized, characterized, and tested for photocatalytic CO_2 reduction. The catalysts show no activity for the reduction, in contrast to the known excellent bipyridine compounds.

The reaction mechanisms were studied successfully with DFT methods, resulting in the proposed new geometry for the production of CO with no carbonate or formate anions. This new geometry does not conflict with known experimental studies, yet avoids three-body mechanistic steps.

Appendix A

Experimental Procedures

Experimental synthesis and characterization data for the compounds discussed in this thesis are shown below by compound number:

A.1 General Methods

Reactions were performed in a glovebox under a nitrogen atmosphere. Solvents were sparged with nitrogen and then dried by passage through a column of activated alumina using an apparatus purchased from Anhydrous Engineering. Deuterated chloroform and deuterated acetonitrile was dried using activated molecular sieves. Rhenium starting materials were purchased from Strem Chemicals and used as received. All other chemicals were purchased from Aldrich and used without further purification. NMR spectra were run on Bruker Avance 400MHz spectrometers with CD_3CN or CDCl_3 as solvent and internal standard. Elemental analyses were performed by Midwest Microlab LLC, Indianapolis IN. Solid state reactions were carried out in a Lindberg Blue M Mini-Mite Tube Furnace (model TF55035A-1). Infrared spectra were collected using an Agilent Technologies Cary FT-IR spectrometer using a diamond ATR attachment. UV-Vis spectra

were collected using a Agilent Technologies Cary 5000 UV-Vis spectrometer. TGA was performed on a TA Q5000 IR instrument: approximately 10-15 mg of each sample was placed in a ceramic sample pan which was heated at a rate of 5°C/min up to 150°C, followed by a rate of 2°C/min to 300°C while being purged with N₂ at a flow rate of 25 mL/min. GC was performed using a HP gas chromatograph with a 15 m CARBON-PLOT column with 0.320 mm inner diameter and 1.50 μ m film in a 40°C oven. The instrument is fitted with a TCD at 220°C.

A.2 Computational Methods

For the UV-Vis and experimental correlation study, the structures of all species were optimized using Gaussian 09⁶⁴ employing the B3LYP^{65,66} exchange-correlation (XC) functional. The LanL2DZ basis set/effective core potential⁶⁷ was used on Re and, the all-electron TZVP basis set^{schaefer1994} for the remaining lighter atoms. Frequency analysis of all structures was used to confirm the nature of the stationary points. Solvent effects were computed using the integral equation formalism variant of the PCM solvation model within Gaussian 09 for both the ground state and excited state TD-DFT calculations with DMSO as the solvent.^{68,69} The UV-Vis absorption spectra were simulated using the Chemissian software.⁷⁰ In these calculations, a pseudo-Voigt band shape was employed with a default average band width at half-height of 2000cm⁻¹.

For the mechanism study, the structures and energies of all species were obtained by using TurboMole 6.5 software^{71,72} with the TPSS meta-GGA XC functional.⁷³ The def2-TZVP basis set was used for all atoms.^{74,75} The TurboMole program contains a number of optimizations to the original DFT algorithms,⁷⁶⁻⁸⁴ decreasing the calculation time without compromising accuracy. Grimme's dispersion correction (version 3) was included in the calculations.⁸⁵ Intermediates and transition states were verified by frequency anal-

ysis.^{dieglmann 2004, 86,87} The effects of solvation was calculated using the Conductor-like Screening Model (COSMO) implemented in TurboMole,⁸⁸ which is a continuum solvation model implicitly surrounding the solute molecule.

A.3 X-ray Crystallography

Crystals were mounted on thin glass fibers using paraffin oil. Prior to data collection crystals were cooled to 200.15K. Data were collected on a Bruker AXS SMART single crystal diffractometer equipped with a sealed Mo tube source (wavelength 0.71073 Å) APEX II CCD detector. Raw data collection and processing were performed with APEX II software package from BRUKER AXS53. Diffraction data for sample **3** was collected with a sequence of 0.5° ω scans at 0, 120, and 240° in ϕ . Due to lower unit cell symmetry in order to ensure adequate data redundancy, diffraction data for **1**, **2** and **8** were collected with a sequence of 0.5° ω scans at 0, 90, 180 and 270° in ϕ . Initial unit cell parameters were determined from 60 data frames with 0.3° ω scan each collected at the different sections of the Ewald sphere. Semi-empirical absorption corrections based on equivalent reflections were applied.⁸⁹ Systematic absences in the diffraction data-set and unit-cell parameters were consistent with triclinic $P\bar{1}$ ($\mathcal{N}^{\mathcal{O}}2$) for compounds **1**, **2** and **8**, monoclinic $C2/c$ ($\mathcal{N}^{\mathcal{O}}15$) for compound **3**. Solutions in the centrosymmetric space groups for all compounds yielded chemically reasonable and computationally stable results of refinement. The structures were solved by direct methods, completed with difference Fourier synthesis, and refined with full-matrix least-squares procedures based on F^2 .

Solutions for **1** and **2** revealed that both these structures contain two compound molecules per asymmetric unit.

Initial refinement results for the compound **1** suggested presence of two non-merohedrally

twinned domains. Two independent orientation matrices were found using CELL_NOW software.⁹⁰ Data set was re-integrated with two independent orientation matrices and consecutive model refinement was performed using HKLF5 format reflection data file. Twinning domain ratio coefficient (BASF) was successfully refined to 0.3794.

On the final model refinement stage for compound **2** thermal motion parameters for coordinated CO (-C(33)=O(3)) and Cl (Cl(2)) moieties as well as presence of unusually strong residual electron density peaks in one of the compound molecules suggested a positional CO / Cl disorder not related by symmetry. Disorder was successfully modeled with refined occupation ratio at one position CO / Cl = 70%:30%. Disorder of the second position was inversed in such way that overall occupancy summed up to one full CO and one full Cl ligands in the first coordination sphere of Re metal center. Set of geometrical (SADI) and thermal motion (SIMU, DELU) restrains were applied to achieve acceptable molecular fragment geometries and thermal motion parameter values.

For all the compounds hydrogen atoms positions were initially assigned from the residual electron density peaks coordinates. However, after initial placement all hydrogen atoms were treated as idealized contributions during the refinement. All scattering factors are contained in several versions of the SHELXTL program library, with the latest version used being v.6.12.⁹¹

A.3.1 X-Ray Structures from Multiple Vantage Points

Multiple views of each x-ray structure discussed in chapter 2.

A.4 (terpy- κ^2 -N,N')Re(CO)₃Cl (**1**)

Re(CO)₅Cl (201 mg, 0.556 mmol) and 2,2':6,2''-terpyridine (129 mg, 0.553 mmol) were mixed in 60 mL of toluene. The reaction mixture was heated to 100°C for 1 hour under N₂. During this time the solution turned a bright red. Upon cooling a yellow precipitate was formed. The solution was filtered, and the solid was washed with diethyl ether, and dried under vacuum. Compound **1** is a bright yellow powder that was isolated in 70 % yield (208 mg). Crystals were obtained from chloroform with addition of a small amount of hexanes as counter solvent. TGA: 8 % mass loss from 240-280°C. FTIR: 2019, 1981, 1889 cm⁻¹ (ν C=O). ¹H NMR (CD₃CN, 400 MHz): δ 9.06 (ddd, J=5.6, 1.7, 0.8 Hz, 1H), 8.77 (ddd, J=4.9 Hz, 1H), 8.49 (tt, J=8.2, 1.0 Hz, 2H), 8.28 (t, J=7.9 Hz, 1H), 8.22 (td, J=8.1, 1.6 Hz, 1H), 7.96 (td, J=7.8, 1.8 Hz, 1H), 7.79 (dt, J=7.8, 1.1 Hz, 1H), 7.80 (dd, J=7.7, 1.0 Hz, 1H), 7.63 (ddd, J=7.6, 5.5, 1.2 Hz, 1H), 7.55 (ddd, J=7.6, 5.0, 1.0 Hz, 1H). Elemental analysis calculated (%) for [C₁₈H₁₁ReClN₃O₃]: C 40.11, H 2.06, N 7.80, found C 39.96, H 2.09, N 7.69.

A.5 (terpy- κ^3 -N,N',N'')Re(CO)₂Cl (**2**)

Compound **1** (101 mg, 0.187 mmol) was placed in a tube furnace and heated to 240°C under N₂ flow for 60 minutes. A black solid was collected (90 mg) at 94 % yield based on the formula for **2**. Crystals were obtained from chloroform with addition of a small amount of hexanes as counter solvent. FTIR: 1872, 1788 cm⁻¹ (ν C=O). ¹H NMR (CD₃CN, 400 MHz): δ 8.93 (ddd, J=5.6, 1.7, 0.7 Hz, 2H), 8.22 (d, J=8.2, 2H), 8.21 (dt, J=8.0, 1.0 Hz, 2H), 8.05 (dd, J=8.4, 7.7 Hz, 1H), 7.91 (t, J=8.1 Hz, 2H), 7.34-7.40 (m, 2H). Elemental analysis calculated (%) for [C₁₇H₁₁ReClN₃O₂]: C 39.96, H 2.17, N 8.22, found C 39.62, H 2.09, N 7.99.

A.6 (terpy- κ^2 -N,N')Re(CO)₃Br (**3**)

Re(CO)₅Br (191 mg, 470 μ mol) and 2,2':6,2''-terpyridine (129 mg, 0.553 mmol) were allowed to react under conditions analogous to the preparation of **1**. A bright yellow powder was obtained, 0.223 g (0.382 mmol, 81 %). FTIR: 2012, 1910, 1886 cm⁻¹ (ν C=O). ¹H NMR (CD₃CN, 400 MHz): δ 9.07 (ddd, J=5.6, 1.6, 0.9 Hz, 1H), 8.77 (ddd, J=4.6, 1.5, 0.8 Hz, 1H), 8.52–8.48 (m, 2H), 8.28 (t, J=7.9 Hz, 1H), 8.21 (td, J=8.0, 1.6 Hz, 1H), 7.97 (td, J=7.8, 1.8 Hz, 1H), 7.80–7.75 (m, 2H), 7.63 (ddd, J=7.6, 5.5, 1.2 Hz, 1H), 7.55 (ddd, J=7.7, 4.9, 1.1 Hz, 1H). Elemental analysis calculated (%) for [C₁₈H₁₁ReBrN₃O₃]: C 37.06, H 1.90, N 7.20, found C 36.94, H 1.92, N 7.00.

A.7 (terpy- κ^3 -N,N',N'')Re(CO)₂Br (**4**)

Compound **3** (182 mg, 0.312 mmol) was placed in an tube furnace and heated to 230°C under N₂ flow for 60 minutes. A black solid was collected, 0.155 mg (0.279 mmol, 89 % yield). Crystals were obtained from chloroform with addition of a small amount of hexanes as counter solvent. FTIR: 1873, 1794 cm⁻¹ (ν C=O). ¹H NMR (CD₃CN, 400 MHz): δ 8.95 (d, J=5.4 Hz, 2H), 8.24 (t, J = 8.1 Hz, 4H), 8.05 (dd, J=8.2, 7.7 Hz, 1H), 7.90 (td, J=7.9, 1.7 Hz, 2H), 7.63 (ddd, J=7.3, 5.5, 1.2 Hz, 2H). Elemental analysis calculated (%) for [C₁₇H₁₁ReBrN₃O₂]: C 36.76, H 2.00, N 7.57, found C 36.66, H 2.00, N 7.50.

A.8 (terpy- κ^2 -N,N')Re(CO)₃OTf (**7**)

To **1** (80 mg, 0.148 mmol), AgCF₃SO₃ (46 mg, 0.179 mmol) was added in 10 mL CH₃CN. The reaction was stirred 24 h and kept dark. Solution was filtered to remove salts, then

reduced in volume. Cold diethyl ether was used to precipitate product. Yellow-grey powder (**7a**) was collected by filtration, yielding 38mg (40 %). Crystals were grown from saturated chloroform with hexanes as countersolvent for X-ray crystallography. FTIR: 2030, 1895, 1890 cm^{-1} (ν C=O), 1280, 1228, 1204 cm^{-1} (ν SO₃). ¹H NMR (CD₃CN, 400 MHz): δ 9.05 (ddd, J=5.5, 1.6, 0.8 Hz, 1H), 8.79 (ddd, J=4.9, 1.8, 1.1 Hz, 1H), 8.57 (dd, J=8.1, 0.9 Hz, 1H), 8.54 (dt, J=8.2, 1.1 Hz, 1H), 8.37 (t, J=7.9 Hz, 1H), 8.31 (td, J=8.0, 1.6 Hz, 1H), 8.03 (td, J=7.7, 1.7 Hz, 1H), 7.87 (dd, J=7.8, 1.0 Hz, 1H), 7.75 (dt, J=7.8, 1.1 Hz, 1H), 7.72 (ddd, J=7.4, 5.9, 1.1 Hz, 1H), 7.61 (ddt, J=7.7, 4.8, 0.5, 0.5 Hz, 1H). Elemental analysis calculated (%) for [C₁₉H₁₁ReN₃O₆F₃S]: C 34.97, H 1.70, N 6.44, found C 31.80, H 1.73, N 5.33.

Alternately, to **1** (72 mg, 0.134 mmol) was added 10 mL CF₃SO₃H (excess) and get temp temperature was increased to for 20 minutes. A black solution was neutralized with addition of 5% Na₂CO₃ in H₂O. Product was extracted with CHCl₃, then dried under vacuum to yield a brown solid (**7b**) (47 mg, 54 %).

A.9 (terpy- κ^3 -N,N',N'')Re(CO)₂OTf (**8**)

To **2** (77 mg, 0.143 mmol), AgSO₃CF₃ (47 mg, 0.183 mmol) was added in 15 mL CH₃CN. Solution was refluxed for 6 h in the dark under N₂ atmosphere. Solution was filtered, then reduced to minimal volume. Cold diethyl ether was added dropwise to precipitate product. Collected by filtration and washed with additional cold ether, yielding 75 mg (120 mmol, 80 %). Crystals grown from saturated methylene chloride, with hexanes as countersolvent for x-ray crystallography. FTIR: 1910, 1829 cm^{-1} (ν C=O), 1259, 1224, 1143 cm^{-1} (ν SO₃). ¹H NMR (CD₃CN, 400 MHz): δ 8.91(ddd, J=5.6, 1.6, 0.7 Hz, 2H), 8.32 (d, J=8.0 Hz, 2H), 8.28 (ddd, J=8.1, 1.4, 0.8 Hz, 2H), 8.19 (dd, J=8.8, 7.4 Hz, 1H), 8.02 (td, J=7.9, 1.5 Hz, 2H) 7.46 (ddd J=7.6, 5.6, 1.3 Hz, 2H). EA Elemental analysis

calculated (%) for $[\text{C}_{18}\text{H}_{11}\text{ReF}_3\text{SN}_3\text{O}_5]$: C 34.62, H 1.78, N 6.37, found C 31.02, H 1.82, N 7.11.

Appendix B

Molecular Orbitals and Energy Diagrams

Frontier Molecular Orbitals (MOs) for each compound discussed in this thesis are collected below. These orbitals are generated with the Chemissian program.⁷⁰

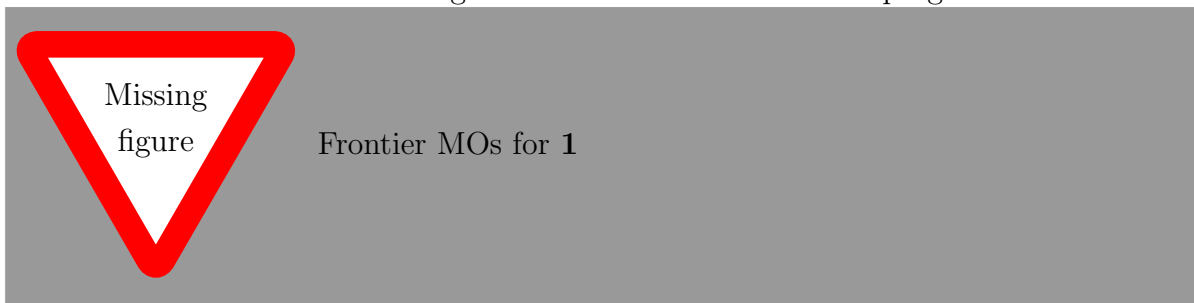


Figure B.1 UV-Vis1

Glossary of Terms

CCDC Cambridge Crystallography Data Centre

DFT Density Functional Theorem

DMF N,N-dimethylformamide

DMSO Dimethylsulfoxide

FTIR Fourier Transform Infrared

GC Gas Chromatography

HOMO Highest Occupied Molecular Orbital

LUMO Lowest Unoccupied Molecular Orbital

MLCT Metal-Ligand Charge Transfer

MO Molecular Orbital

NMR Nuclear Magnetic Resonance

TCD Thermal Conductivity Detector

TD-DFT Time Dependant Density Functional Theorem

TEA Triethylamine

TEOA Triethanolamine

TGA Thermogravimetric Analysis

Bibliography

1. Zeise, W. C. *J. Physik und Chemie (Schweigger)* **1831**, *62*, 393–441.
2. Hunt, L. B. *Platinum Metals Review* **1984**, *28*, 76–83.
3. Griess, J. P.; Martius, C. A. *Compt rendus*. **1861**, *53*, 922–925.
4. Birnbaum, K. *Ann. Chem. (Liebig)* **1868**, *145*, 67–77.
5. Small, B. L.; Brookhart, M. *Journal of the American Chemical Society* **1998**, *120*, 7143–7144.
6. Small, B. L.; Brookhart, M.; Bennett, A. M. A. *Journal of the American Chemical Society* **1998**, *120*, 4049–4050.
7. J. P. Britovsek, G.; C. Gibson, V.; J. McTavish, S.; A. Solan, G.; J. P. White, A.; J. Williams, D.; J. P. Britovsek, G.; S. Kimberley, B.; J. Maddox, P. *Chem. Commun.* **1998**, 849–850.
8. Britovsek, G. J. P.; Bruce, M.; Gibson, V. C.; Kimberley, B. S.; Maddox, P. J.; Mastroianni, S.; McTavish, S. J.; Redshaw, C.; Solan, G. A.; Strömberg, S.; White, A. J. P.; Williams, D. J. *Journal of the American Chemical Society* **1999**, *121*, 8728–8740.
9. Gibson, V. C.; Redshaw, C.; Solan, G. A. *Chemical Reviews* **2007**, *107*, PMID: 17488059, 1745–1776.
10. Boudier, A.; Breuil, P.-A. R.; Magna, L.; Olivier-Bourbigou, H.; Braunstein, P. *Chem. Commun.* **2014**, *50*, 1398–1407.
11. Dudle, B.; Rajesh, K.; Blacque, O.; Berke, H. *Journal of the American Chemical Society* **2011**, *133*, 8168–8178.
12. Jain, K. R.; Herrmann, W. A.; Kühn, F. E. *Coordination Chemistry Reviews* **2008**, *252*, Chiral Catalysis, 556–568.
13. Kuninobu, Y.; Takai, K. *Chemical Reviews* **2011**, *111*, 1938–1953.
14. Bartholoma, M.; Valliant, J.; Maresca, K. P.; Babich, J.; Zubieta, J. *Chem. Commun.* **2009**, 493–512.
15. Schibli, R.; Schubiger, A. **2002**, *29*, 1529–1542.

16. Coogan, M.; Fernández-Moreira, V.; Kariuki, B.; Pope, S.; Thorp-Greenwood, F. *Angewandte Chemie International Edition* **2009**, *48*, 4965–4968.
17. Giordano, P. J.; Wrighton, M. S. *Journal of the American Chemical Society* **1979**, *101*, 2888–2897.
18. Fredericks, S. M.; Luong, J. C.; Wrighton, M. S. *Journal of the American Chemical Society* **1979**, *101*, 7415–7417.
19. Sacksteder, L.; Zipp, A. P.; Brown, E. A.; Streich, J.; Demas, J. N.; DeGraff, B. A. *Inorganic Chemistry* **1990**, *29*, 4335–4340.
20. Caspar, J. V.; Meyer, T. J. *The Journal of Physical Chemistry* **1983**, *87*, 952–957.
21. Yam, V. W.-W. *Chem. Commun.* **2001**, 789–796.
22. Feliz, M.; Rodriguez-Nieto, F.; Ruiz, G.; Wolcan, E. *Journal of Photochemistry and Photobiology A: Chemistry* **1998**, *117*, 185–192.
23. Ruiz, G.; Wolcan, E.; Feliz, M. *Journal of Photochemistry and Photobiology A: Chemistry* **1996**, *101*, 119–125.
24. Lin, R.; Fu, Y.; Brock, C. P.; Guarr, T. F. *Inorganic Chemistry* **1992**, *31*, 4346–4353.
25. Hino, J. K.; Della Ciana, L.; Dressick, W. J.; Sullivan, B. P. *Inorganic Chemistry* **1992**, *31*, 1072–1080.
26. Walters, K. A.; Kim, Y.-J.; Hupp, J. T. *Inorganic Chemistry* **2002**, *41*, 2909–2919.
27. Striplin, D.; Crosby, G. *Coordination Chemistry Reviews* **2001**, *211*, 163–175.
28. Martin, T. A.; Ellul, C. E.; Mahon, M. F.; Warren, M. E.; Allan, D.; Whittlesey, M. K. *Organometallics* **2011**, *30*, 2200–2211.
29. Abel, E. W.; Wilkinson, G. *J. Chem. Soc.* **1959**, 1501–1505.
30. Kirkham, W. J.; Osborne, A. G.; Nyholm, R. S.; Stiddard, M. H. B. *J. Chem. Soc.* **1965**, 550–553.
31. Zingales, F.; Sartorelli, U.; Trovati, A. *Inorganic Chemistry* **1967**, *6*, 1246–1248.
32. Gamelin, D. R.; George, M. W.; Glyn, P.; Grevels, F.-W.; Johnson, F. P. A.; Klotzbuecher, W.; Morrison, S. L.; Russell, G.; Schaffner, K.; Turner, J. J. *Inorganic Chemistry* **1994**, *33*, 3246–3250.
33. Martí, A. A.; Mezei, G.; Maldonado, L.; Paralitici, G.; Raptis, R. G.; Colón, J. L. *European Journal of Inorganic Chemistry* **2005**, *2005*, 118–124.
34. Morse, D. L.; Wrighton, M. S. *Journal of the American Chemical Society* **1976**, *98*, 3931–3934.
35. Giordano, P. J.; Fredericks, S. M.; Wrighton, M. S.; Morse, D. L. *Journal of the American Chemical Society* **1978**, *100*, 2257–2259.

36. Granifo, J.; Bird, S. J.; Orrell, K. G.; Osborne, A. G.; Šik, V. *Inorganica Chimica Acta* **1999**, *295*, 56–63.
37. Orrell, K. G.; Osborne, A. G.; Šik, V.; da Silva, M. W.; Hursthouse, M. B.; Hibbs, D. E.; Malik, K. A.; Vassilev, N. G. *Journal of Organometallic Chemistry* **1997**, *538*, 171–183.
38. Abel, E. W.; Dimitrov, V. S.; Long, N. J.; Orrell, K. G.; Osborne, A. G.; Pain, H. M.; Sik, V.; Hursthouse, M. B.; Mazid, M. A. *J. Chem. Soc., Dalton Trans.* **1993**, 597–603.
39. Gong, X.; Ng, P. K.; Chan, W. K. *Advanced Materials* **1998**, *10*, 1337–1340.
40. Lo, K. K.-W.; Louie, M.-W.; Zhang, K. Y. *Coordination Chemistry Reviews* **2010**, *254*, 18th International Symposium on the Photochemistry and Photophysics of Coordination Compounds Sapporo, 2009, 2603–2622.
41. Lin, T.-P.; Chen, C.-Y.; Wen, Y.-S.; Sun, S.-S. *Inorganic Chemistry* **2007**, *46*, 9201–9212.
42. Slone, R. V.; Yoon, D. I.; Calhoun, R. M.; Hupp, J. T. *Journal of the American Chemical Society* **1995**, *117*, 11813–11814.
43. D. Beer, P.; Timoshenko, V.; Maestri, M.; Passaniti, P.; Balzani, V. *Chem. Commun.* **1999**, 1755–1756.
44. Beer, P. D.; Hayes, E. J. *Coordination Chemistry Reviews* **2003**, *240*, 35 Years of Synthetic Anion Receptor Chemistry 1968–2003, 167–189.
45. Amoroso, A. J.; Arthur, R. J.; Coogan, M. P.; Court, J. B.; Fernandez-Moreira, V.; Hayes, A. J.; Lloyd, D.; Millet, C.; Pope, S. J. A. *New J. Chem.* **2008**, *32*, 1097–1102.
46. Amoroso, A. J.; Coogan, M. P.; Dunne, J. E.; Fernandez-Moreira, V.; Hess, J. B.; Hayes, A. J.; Lloyd, D.; Millet, C.; Pope, S. J. A.; Williams, C. *Chem. Commun.* **2007**, 3066–3068.
47. Hawecker, J.; Lehn, J.-M.; Ziessel, R. *J. Chem. Soc., Chem. Commun.* **1983**, 536–538.
48. Hawecker, J.; Lehn, J.-M.; Ziessel, R. *Helvetica Chimica Acta* **1986**, *69*, 1990–2012.
49. Takeda, H.; Ishitani, O. *Coordination Chemistry Reviews* **2010**, *254*, Inorganic Reaction Mechanisms A Tribute to Ralph Pearson on the occasion of his 90th birthday, 346–354.
50. Christensen, P.; Hamnett, A.; Muir, A. V. G.; Timney, J. A. *J. Chem. Soc., Dalton Trans.* **1992**, 1455–1463.
51. Sullivan, B. P.; Bolinger, C. M.; Conrad, D.; Vining, W. J.; Meyer, T. J. *J. Chem. Soc., Chem. Commun.* **1985**, 1414–1416.
52. Caulton, K. G. *European Journal of Inorganic Chemistry* **2012**, *2012*, 435–443.

53. Jurca, T.; Chen, W.-C.; Michel, S.; Korobkov, I.; Ong, T.-G.; Richeson, D. S. *Chemistry – A European Journal* **2013**, *19*, 4278–4286.
54. Juris, A.; Campagna, S.; Bidd, I.; Lehn, J. M.; Ziessel, R. *Inorganic Chemistry* **1988**, *27*, 4007–4011.
55. Black, D. R.; Hightower, S. E. *Inorganic Chemistry Communications* **2012**, *24*, 16–19.
56. Russell, S. K.; Darmon, J. M.; Lobkovsky, E.; Chirik, P. J. *Inorganic Chemistry* **2010**, *49*, PMID: 20143847, 2782–2792.
57. Tondreau, A. M.; Atienza, C. C. H.; Weller, K. J.; Nye, S. A.; Lewis, K. M.; Delis, J. G. P.; Chirik, P. J. *Science* **2012**, *335*, 567–570.
58. Buckingham, D.; Dwyer, F.; Goodwin, H.; Sargeson, A. *Australian Journal of Chemistry* **Jan. 1964**, *17*, 315–324.
59. Compain, J.-D.; Bourrez, M.; Haukka, M.; Deronzier, A.; Chardon-Noblat, S. *Chem. Commun.* **2014**, *50*, 2539–2542.
60. Allen, F. H. *Acta Crystallographica Section B* **2002**, *58*, 380–388.
61. Koike, K.; Okoshi, N.; Hori, H.; Takeuchi, K.; Ishitani, O.; Tsubaki, H.; Clark, I. P.; George, M. W.; Johnson, F. P. A.; Turner, J. J. *Journal of the American Chemical Society* **2002**, *124*, 11448–11455.
62. Machan, C. W.; Sampson, M. D.; Chabolla, S. A.; Dang, T.; Kubiak, C. P. *Organometallics* **2014**, *Accepted Article*, DOI: 10.1021/om500044a.
63. Shaver, R. J.; Rillema, D. P. *Inorganic Chemistry* **1992**, *31*, 4101–4107.
64. Frisch, M. J. et al. Gaussian 09 Revision D.01., Gaussian Inc. Wallingford CT 2009.
65. Becke, A. D. *The Journal of Chemical Physics* **1993**, *98*, 5648–5652.
66. Lee, C.; Yang, W.; Parr, R. G. *Phys. Rev. B* **1988**, *37*, 785–789.
67. Hay, P. J.; Wadt, W. R. *The Journal of Chemical Physics* **1985**, *82*, 299–310.
68. Tomasi, J.; Mennucci, B.; Cammi, R. *Chemical Reviews* **2005**, *105*, 2999–3094.
69. Scalmani, G.; Frisch, M. J.; Mennucci, B.; Tomasi, J.; Cammi, R.; Barone, V. *The Journal of Chemical Physics* **2006**, *124*, 094107, –.
70. Skripnikov, L. Chemissian, a computer program to analyze and visualize quantum-chemical calculations., www.chemissian.com, 2013.
71. TURBOMOLE V6.5, a development of University of Karlsruhe and Forschungszentrum Karlsruhe GmbH., available from www.turbomole-gmbh.com, 2013.
72. Ahlrichs, R.; Bär, M.; Häser, M.; Horn, H.; Kölmel, C. *Chemical Physics Letters* **1989**, *162*, 165–169.
73. Tao, J.; Perdew, J. P.; Staroverov, V. N.; Scuseria, G. E. *Phys. Rev. Lett.* **2003**, *91*, 146401.

74. Schäfer, A.; Huber, C.; Ahlrichs, R. *The Journal of Chemical Physics* **1994**, *100*, 5829–5835.
75. Weigend, F.; Ahlrichs, R. *Phys. Chem. Chem. Phys.* **2005**, *7*, 3297–3305.
76. Haase, F.; Ahlrichs, R. *Journal of Computational Chemistry* **1993**, *14*, 907–912.
77. Treutler, O.; Ahlrichs, R. *The Journal of Chemical Physics* **1995**, *102*, 346–354.
78. Eichkorn, K.; Weigend, F.; Treutler, O.; Ahlrichs, R. **1997**, *97*, 119–124.
79. Eichkorn, K.; Treutler, O.; Öhm, H.; Häser, M.; Ahlrichs, R. *Chemical Physics Letters* **1995**, *242*, 652–660.
80. Sierka, M.; Hogeekamp, A.; Ahlrichs, R. *The Journal of Chemical Physics* **2003**, *118*, 9136–9148.
81. Deglmann, P.; May, K.; Furche, F.; Ahlrichs, R. *Chemical Physics Letters* **2004**, *384*, 103–107.
82. Weigend, F. *Phys. Chem. Chem. Phys.* **2002**, *4*, 4285–4291.
83. Von Arnim, M.; Ahlrichs, R. *Journal of Computational Chemistry* **1998**, *19*, 1746–1757.
84. Ahlrichs, R. *Phys. Chem. Chem. Phys.* **2004**, *6*, 5119–5121.
85. Grimme, S.; Antony, J.; Ehrlich, S.; Krieg, H. *The Journal of Chemical Physics* **2010**, *132*, 154104, –.
86. Deglmann, P.; Furche, F.; Ahlrichs, R. *Chemical Physics Letters* **2002**, *362*, 511–518.
87. Grimme, S.; Furche, F.; Ahlrichs, R. *Chemical Physics Letters* **2002**, *361*, 321–328.
88. Klamt, A.; Schuurmann, G. *J. Chem. Soc., Perkin Trans. 2* **1993**, 799–805.
89. Blessing, R. H. *Acta Crystallographica Section A* **1995**, *51*, 33–38.
90. Sheldrick, G. CellNow., Bruker AXS: Madison, WI, 2004.
91. Sheldrick, G. M. *Acta Crystallographica Section A* **2008**, *64*, 112–122.

Todo list

Rewrite to more verbose	3
Take out spoilers	5
Figure: bidentate scheme	8
check that value	9
Further discuss TGA & terdentate rxn to build a space to put in scheme2	9
Figure: terdentate scheme2	9
Figure: anion exchange reaction schemes	10
ref	10
Figure: anion exchange reaction schemes	10
Figure: S6 from paper, nmr of 2,3,4	12
check compounds & spectra	12
Get paper citation	12
Titel's Thesis citation	12
Figure: S5 from paper, showing bi-terdentate	12
check compounds & spectra	13
Put in nmr peak values	13
Figure: expanded terpy	13
why poor, show an ok result & discuss	13
the rest of structures	13
ref	14
not done	17
Get IR info	24
Figure: Some UV-Vis from the paper	25
This will be longer. Should be lots of discussion about results differences. I need to a)highlight the importance of anion exchange, and then b) highlight the importance of bidentate vs. terdentate	25
This will be longer. Should be lots of discussion about results differences. I need to a)highlight the importance of anion exchange, and then b) highlight the importance of bidentate vs. terdentate	27
Conclusion shows that manipulations can be done, this affects the photophysical properties of the compounds and may affect the photochemical	27
check ref names	28

a few references	28
refer to these as well. Red Light paper?	28
references, Morris, JACS dimer, mech. basis	28
more	31
Figure: Three mechanistic pathway quick	32
Make mechanism (or get morris?)	32
Ref. Sullivan and Gilbert	32
refs	32
fluorescence tests on 1,2	33
ref lehn88?	33
Set up a detailed naming scheme that will work for the entire chapter, likely having to start with M## or similar motif.	33
computationally back it up	33
pathway numbrs as well	33
Figure: Three mechanistic energy comparison	34
SOLVE ENERGY	34
get temp	42
Figure: Frontier MOs for 1	44